

Extreme value and record statistics in heavy-tailed processes with long-range memory

Aicko Y. Schumann¹, Nicholas R. Moloney^{1,2} and Jörn Davidsen¹

Abstract. Extreme events are an important theme in various areas of science because of their typically devastating effects on society and their scientific complexities. The latter is particularly true if the underlying dynamics does not lead to independent extreme events as often observed in natural systems. Here, we focus on this case and consider stationary stochastic processes that are characterized by long-range memory and heavy-tailed distributions, often called fractional Lévy noise. While the size distribution of extreme events is not affected by the long-range memory in the asymptotic limit and remains a Fréchet distribution, there are strong finite-size effects if the memory leads to persistence in the underlying dynamics. Moreover, we show that this persistence is also present in the extreme events, which allows one to make a time-dependent hazard assessment of future extreme events based on events observed in the past. This has direct applications in the field of space weather as we discuss specifically for the case of the solar power influx into the magnetosphere. Finally, we show how the statistics of records, or record-breaking extreme events, is affected by the presence of long-range memory.

1. Introduction

History often turns on extreme events — rare occurrences of extraordinary nature — be they man-made or natural. Examples are global financial crises, military strikes, radical political events, or natural disasters such as floods, droughts and earthquakes. Extreme events are often associated with catastrophes, and the word ‘extreme’ is sometimes substituted by ‘freak’ to suggest something unnatural and undesirable. Generally, the economic and social consequences of extreme events are a matter of enormous concern. In particular, the ever increasing economic and human losses from natural hazards underscore the urgency for improved understanding of extreme events to develop effective strategies to reduce their impact.

The surprisingly high likelihood of extreme events is actually a key attribute of many complex systems, in both natural and man-made environments (see, e.g., [Albeverio *et al.*, 2006; Bunde *et al.*, 2002; Embrechts *et al.*, 2004; Galambos *et al.*, 1994; Sornette, 2006]). In particular, we know that records must be broken in the future, so if a flood design is based on the worst case of the past, then we are still not prepared for all possible floods in the future. The classic approach to studying the probability of extreme events has been to assume independent and identically distributed (iid) event sizes. This has led to a powerful statistical theory (see, e.g., [Embrechts *et al.*, 2004; Coles, 2007; de Haan and Ferreira, 2006]), which has been successfully applied in many cases (see, e.g., [Easterling *et al.*, 2000; Glaser and Stangl, 2004; van den Brink and Können, 2008]). The latter is also related to the fact that some parts of the theory — for example, the limit distributions of block maxima — can be extended to a wide class of dependent stationary stochastic processes and their associated time series [Berman, 1964; Leadbetter *et al.*, 1983; Leadbetter and

Rootzén, 1988; Samorodnitsky, 2004]. However, we are still far away from a general understanding of extreme events generated by such dependent processes, which are abundant in nature. Complicating factors typically include slow convergence and strong finite-size effects [Gyöngyi *et al.*, 2008], as well as nonlinear correlations [Bogachev *et al.*, 2007].

Strikingly, one often encounters dependence in the form of long-range persistence in recordings taken from natural systems. Persistence is defined as the tendency that subsequent values in a time series are similar: large values tend to be followed by large values and small values tend to be followed by small values. Such behavior has been reported for water levels in rivers [Hurst, 1951] and in river runoff records [Kantelhardt *et al.*, 2003, 2006], in climatological temperature recordings [Koscielny-Bunde *et al.*, 1998; Pelletier and Turcotte, 1997; Huybers and Curry, 2006] and for temperature fluctuations in oceans [Monetti *et al.*, 2002], as well as in marine data [Roman *et al.*, 2008], to name only a few examples.

The theoretical studies of the extreme value statistics of stationary stochastic processes exhibiting long-range persistence have mainly focused on processes with Gaussian distributed event sizes. In this and related cases, the limit distribution of the block maxima is the same as in the iid case — a Gumbel distribution [Berman, 1964; Eichner *et al.*, 2006]. Similar results have been obtained for beta-distributed random variables, in which case the Gumbel distribution is replaced by the Weibull distribution [Moloney and Davidsen, 2009]. Meanwhile, for distributions with power-law tails the block maxima for iid events are Fréchet distributed [Embrechts *et al.*, 2004], and this is even true for a certain class of dependent sequences [Leadbetter *et al.*, 1983; Leadbetter and Rootzén, 1988]. Power-law tails imply that there is no “typical” event size and that indeed event sizes vary over many orders of magnitude. Many natural systems even obey distributions of Pareto-like (power-law-like) heavy tails, such that the second moment of the distribution is not defined. In space physics, such heavy-tailed distributions have been used to model e.g. magnetic field line transport [Pommois *et al.*, 1998], fluctuations in various solar wind parameters [Hnat *et al.*, 2003; Bruno *et al.*, 2004; Zaslavsky *et al.*, 2008] and auroral indices [Watkins *et al.*, 2005; Zaslavsky *et al.*, 2008]. Other examples include, size distributions in geology [Caers *et al.*, 1999], meteorology [Taqq, 1987], or sediments [Painter and Paterson, 1994].

¹Complexity Science Group, Department of Physics and Astronomy, University of Calgary, 2500 University Dr. NW, Calgary, Alberta T2N 4L1, Canada.

²Max Planck Institute for the Physics of Complex Systems, Nöthnitzer Str. 38, 01187 Dresden, Germany.

Here, we study the extreme value statistics of exactly those stationary stochastic processes that are characterized by persistent (or anti-persistent) long-range memory and heavy tails. These processes are sometimes called fractional Lévy noise or linear stable fractional noise — see [Watkins *et al.*, 2009; Moloney and Davidsen, 2010] for discussions and further references. Specifically, we consider those symmetric α -stable distributed processes ($0 < \alpha < 2$) that are characterized by a self-similarity index H with $0 < H < 1$. These are particularly relevant in the context of the solar wind as discussed, for example, by Moloney and Davidsen [2010] for the energy influx into the magnetosphere, which is captured by the Akasofu ϵ parameter. While it is known that the limit distribution of the block maxima remains a Fréchet distribution for all α and H [Samorodnitsky, 2004], we systematically quantify the finite size corrections. As expected, they are particularly pronounced for strong persistence but they also play a role in the presence of anti-persistence. Moreover, we show that the conditional block maxima distributions deviate significantly from the unconditional distribution for small block sizes. This history dependence allows one to make a time-dependent hazard assessment of the value of the next block maximum based on the previous one. We also show how the statistics of records, or record-breaking extreme events, is affected by the presence of long-range memory and, thus, extend very recent results for the Gaussian distributed case [Newman *et al.*, 2010]. Finally, we apply the time-dependent hazard assessment and the record analysis to the ϵ time series derived from ACE spacecraft measurements for the years 2000 – 2007.

The paper is organized as follows: First we review basic properties and limit theorems of (maximum) extreme value statistics in Sect. 2, followed by record statistics in Sect. 3. We then describe α -stable- or Lévy distributions and discuss the generation of stationary symmetric α -stable distributed processes with long-range memory in Sect. 4. The presentation of our numerical results can be subdivided into two parts. While we focus on estimating the extreme value statistics of these processes including simple block maxima and conditional block maxima in Sects. 5.1 and 5.2, their record statistics is presented in Sect. 5.3. Section 6 discusses the application of the introduced methodology to the solar power influx into the Earth's magnetosphere. Finally we conclude in Sect. 7.

2. Classical Extreme Value Statistics

In classical extreme value statistics one considers sets of independent identically distributed random variables $\{X_1, X_2, \dots, X_n\}$, each drawn from the same cumulative distribution function $F(x)$. $F(x)$ can typically be represented by a unique probability density function $P(x)$. A time series $\{x_i\}_{i=1, \dots, n}$ can then be understood as one possible realization of the set of random variables, $\{X_1 = x_1, X_2 = x_2, \dots, X_n = x_n\}$, following this density function $P(x)$. The distribution of the (block) maximum or extreme value $M_n = \max\{X_1, \dots, X_n\}$ is given by

$$\begin{aligned} \Pr(M_n \leq m) &= \Pr(X_1 \leq m, \dots, X_n \leq m) \\ &= \prod_{i=1}^n \Pr(X_i \leq m) = F^n(m). \end{aligned} \quad (1)$$

The *Fischer-Tipett-Gnedenko theorem* states that if there exists a renormalization sequence $\{a_n, b_n\}$, $a_n \in \mathbb{R}^+$ and $b_n \in \mathbb{R}$, such that

$$\lim_{n \rightarrow \infty} \Pr\left(\frac{M_n - b_n}{a_n} \leq m\right) \stackrel{d}{=} G(m), \quad (2)$$

where $G(m)$ is non-degenerate and d means convergence in distribution, then the asymptotic limit distribution $G(m)$ belongs to one of the following three function families [Coles, 2007]:

$$G_{\text{Gumbel}}(m) = \exp\left\{-\exp\left\{-\left(\frac{m-b}{a}\right)\right\}\right\} \quad (3a)$$

$$G_{\text{Fréchet}}(m) = \begin{cases} 0 & : m \leq b \\ \exp\left\{-\left(\frac{m-b}{a}\right)^{-\alpha}\right\} & : m > b \end{cases} \quad (3b)$$

$$G_{\text{Weibull}}(m) = \begin{cases} \exp\left\{-\left(-\left(\frac{m-b}{a}\right)\right)^\alpha\right\} & : m < b \\ 1 & : m \geq b. \end{cases} \quad (3c)$$

Here, $a \in \mathbb{R}^+$, $b \in \mathbb{R}$ and $\alpha > 0$. As evident from Eq. (1), the exact limiting distribution is determined by $F(x)$ and, thus, $P(x)$.

If, for instance, $P(x)$ corresponds to the normal distribution or the exponential distribution, the limit distribution of the (block) maxima or extreme values follows a *Gumbel* distribution (Eq. (3a)). In cases where $P(x)$ exhibits power law right tails (Pareto-like tails), i. e., $\overline{P}(x) \sim L(x)x^{-1-\alpha}$ where $\overline{P}(x)$ is the tail of the distribution $P(x)$, $L(x)$ is some slowly varying function, the limit distribution of the (block) maximum or extreme value approaches the *Fréchet* distribution (Eq. (3b)) with the same $\alpha > 0$. Finally, the limit distribution of the maximum falls into the *Weibull* class for some distributions with bounded right tails, such as the beta distribution (Eq. (3c)). Note that the convergence to one of the three distributions in Eq. (3) requires the condition in Eq. (2) to be valid. For example, the condition in Eq. (2) is not generally satisfied for the Poisson distribution, the geometric distribution, or the negative binomial distribution [de Haan and Ferreira, 2006; Embrechts *et al.*, 1997].

All three extreme value distributions in Eqs. (3) can be written in a compact form in terms of the generalized extreme value distribution (GEV)

$$G(z) = \exp\left\{-\left[1 + \xi\left(\frac{z-\mu}{\sigma}\right)\right]_+^{-1/\xi}\right\} \quad (4)$$

where $+$ indicates the constraint $[1 + \xi(\frac{z-\mu}{\sigma})] > 0$. The parameters are the *shape parameter* ξ , $\xi \in \mathbb{R}$, the *scale parameter* σ , $\sigma \in \mathbb{R}^+$, and the *location parameter* μ , $\mu \in \mathbb{R}$. The shape parameter ξ determines the distribution family: $\xi = 0$ (interpreted as $\lim_{\xi \rightarrow 0}$) indicates the Gumbel class (Eq. (3a)), $\xi > 0$ the Fréchet class (Eq. (3b)), and $\xi < 0$ the Weibull class (Eq. (3c)).

In this paper, we exclusively focus on symmetric α -stable distributed processes with long-range memory, for which the block maxima asymptotically converge in distribution to the Fréchet extreme value distribution in Eq. (3b) [Samorodnitsky, 2004].

3. Classical Record Statistics

The field of record statistics is closely related to extreme value statistics since records can be considered as a special type of extreme values: Records are simply record-breaking extreme values, i.e., the sequence of extreme values for increasing n . Studies of record values and record times started with the pioneering work by Chandler [1952] followed by important contributions by Rény [1962]. For a comprehensive overview and a historic summary we refer to [Glick, 1978] and [Neuzorov, 2001] and references therein. The classical theory of records is based on the assumption of iid random variables and has been successfully extended and applied to many natural systems, including earthquakes [Davidsen *et al.*, 2006, 2008; Van Aalsburg *et al.*, 2010; Vasudevan *et al.*, 2010; Peixoto *et al.*, 2010], climate dynamics [Schmittmann and Zia, 1999; Benestad,

2003; Redner and Petersen, 2006; Benestad, 2008; Newman et al., 2010; Wergen and Krug, 2010], hydrology [Vogel et al., 2001] and evolution [Sibani and Jensen, 2009].

Specifically, let again $\{X_1, X_2, \dots, X_R\}$ be a sequence of iid random variables with a common continuous distribution $F(x)$. One possible realization of the set of random variables may then be given by the time series $\{x_i\}_{i=1, \dots, R} = \{x_1, x_2, \dots, x_R\}$. We denote X_m as an (upper) record if $X_m = \max\{X_1, \dots, X_m\}$ for $m \leq R$. As illustrated in Fig. 1, the set of records for a given realization is trivially ordered and the index m at which the k -th record occurs is defined as the k -th record time, T_k . Obviously, $T_1 = 1$ and $T_{k \geq 2} = \min\{j \leq R : X_j > X_{T_{k-1}}\}$. Thus, $T_{k \geq 1}$ as well as the number of records after a time $t \leq R$ in a block of size R , N_t , are random variables themselves.

Interestingly, many statistical properties of records are identical for all sequences of iid random variables $\{X_i\}_{i=1, \dots, R}$ and, thus, independent of the distribution $F(x)$. This includes the expected number of records and their variance. To see this, it is important to realize that each $X_{k \leq m}$ has the same probability of being the maximum, which is simply given by

$$P(X_k = \max\{X_1, \dots, X_m\}) = 1/m. \quad (5)$$

Thus, this is in particular the probability that X_m is a record, which allows one immediately to calculate the expected number of records after a time t and their variance [Glick, 1978]:

$$\begin{aligned} E(N_t) &= \sum_{m=1}^t P(X_m = \max\{X_1, \dots, X_m\}) \\ &= \sum_{m=1}^t 1/m = \ln(t) + \gamma + \mathcal{O}(1/t) \end{aligned} \quad (6a)$$

$$\begin{aligned} \text{Var}(N_t) &= \sum_{m=1}^t \frac{1}{m} - \sum_{m=1}^t \frac{1}{m^2} \\ &= \ln(t) + \gamma + \mathcal{O}(1/t) - \pi^2/6, \end{aligned} \quad (6b)$$

where $\gamma = 0.577 \dots$ is the Euler-Mascheroni constant.

Note, that there are other properties of records, as for instance the distribution of occurrence times of the k -th records [Glick, 1978], that are also independent of the distribution of $\{X_i\}_{i=1, \dots, R}$ but will not be further discussed here. In contrast to the above distribution-independent properties, results involving actual record values do generally depend on the distribution $F(x)$ [Neuzorov, 2001; Redner and Petersen, 2006].

4. Heavy-tailed processes with long-range memory

A prototype of stationary stochastic processes with heavy-tailed distributions are α -stable processes. A random variable X is called stable if any set of independent copies of X , $\{X_1, \dots, X_n\}$, obeys

$$X_1 + \dots + X_n \stackrel{d}{=} c_n X + d_n \quad (7)$$

for some $c_n \in \mathbb{R}^+$ and $d \in \mathbb{R}$ [Embrechts and Schmidli, 1994]. This property implies that the shape of the distribution remains invariant if sums over the random variable are considered. If $d_n = 0$, X is referred to as strictly stable, and X is symmetric if $X \stackrel{d}{=} -X$. A generalized central limit theorem proves that all distributions that have a probability density function $P(x)$ with an associated Fourier transform or characteristic function of the form

$$\varphi_{\alpha, \beta, \delta, \gamma}(t) = \begin{cases} \exp \left\{ it\delta - \gamma^\alpha |t|^\alpha \left(1 - i\beta \operatorname{sgn}(t) \tan \left(\frac{\pi\alpha}{2} \right) \right) \right\} \\ \exp \left\{ it\delta - \gamma |t| \left(1 + \frac{2}{\pi} i\beta \operatorname{sgn}(t) \ln |t| \right) \right\} \end{cases} \quad (8)$$

are stable [Samorodnitsky and Taqqu, 1994]. In particular, the constants c_n are not arbitrary but scale as $n^{1/\alpha}$ with $\alpha \in (0, 2]$, and hence, the corresponding distributions are called α -stable (α S) distributions. In Eq. (8), the *characteristic exponent* or *index of stability* $\alpha \in (0, 2]$, the *skewness parameter* $\beta \in [-1, 1]$, and the *scale parameter* $\gamma \in \mathbb{R}^+$ describe the shape of the distribution while $\delta \in \mathbb{R}$ is the *location parameter*. Since many of these α S distributions do not possess a finite mean and standard deviation, these quantities are typically not used to characterize these distributions.

For symmetric α -stable (SaS) distributions, the skewness parameter obeys $\beta = 0$. In particular, the Gaussian distribution $\mathcal{N}(\mu, \sigma^2)$ is SaS with $(\alpha = 2, \beta = 0, \gamma = \sigma/\sqrt{2}, \delta = \mu)$. Throughout this paper we will only focus on SaS distributed time series and set without loss of generality the location parameter δ to zero. We will further normalize our time series to ensure $\gamma = 1$ (see Sect. 4.2). Hence, Eq. (8) reduces to the simple form

$$\varphi_\alpha(t) = \exp \{-|t|^\alpha\}. \quad (9)$$

While even in this case an analytical form of $P(x)$ is typically not known, the asymptotic behavior for $\alpha \in (0, 2)$ is characterized by *Pareto-like* power-law tails with $\bar{P}(x) \sim x^{-1-\alpha}$ [Sornette, 2006]. Consequently, the variance of all non-Gaussian α S distributions with $\alpha < 2$ is undefined. In addition, the distribution's mean value is undefined for $\alpha < 1$.

4.1. Long-range memory in symmetric α -stable processes

For a sequence of identically but *not* independently distributed random variables $\{X_1, X_2, \dots, X_n\}$ with a common continuous distribution $F(x)$, the associated realizations or stationary time series $\{x_i\}_{i=1, \dots, n} = \{x_1, x_2, \dots, x_n\}$ are typically characterized by non-trivial correlations. One particular example is the presence of long-range linear auto-correlations. These can be described by three equivalent definitions, namely a power-law behavior in (i) the auto-correlation function with correlation exponent $0 < \gamma < 1$, $C(s) \sim s^{-\gamma}$, (ii) the power spectrum with spectral exponent $0 < \beta < 1$, $P(f) \sim f^{-\beta}$, as well as (iii) the fluctuation function with (monofractal) fluctuation exponent $h(2)$, $F(s) \sim s^{h(2)}$ for scales s , frequencies f , and $1 - \beta = \gamma = 2 - 2h(2)$; for a comprehensive definition and discussion, see [Schumann, 2011] and references therein.

While such long-range linear auto-correlations imply long-range persistence, the reverse is not necessarily true. In particular, the above definitions require that a finite variance exists which is not the case for α -stable processes with $\alpha < 2$ as discussed above. Thus, one has to use an alternative way to quantify persistence and long-range memory in general for such processes. One possibility is to define persistence based on the closely related phenomenon of self-similarity. A (continuous) stochastic process $X = \{X(t), t \in \mathbb{R}\}$ is called self-similar with a self-similarity parameter $H > 0$ if $\forall \kappa > 0$, $t \in \mathbb{R}$, [Embrechts and Makoto, 2002],

$$\{X(\kappa t)\} \stackrel{d}{=} \{\kappa^H X(t)\}. \quad (10)$$

It can be further shown that for self-similar SaS distributed processes $X_{H, \alpha}$ with $0 < H < 1$, long-range persistence is achieved for $H > 1/\alpha$, while $H = 1/\alpha$ corresponds to the uncorrelated case and anti-persistence emerges for $H < 1/\alpha$ [Stoev and Taqqu, 2004]. Thus, persistent behavior can only

be observed if $1 < \alpha < 2$ and we focus on this range of α values in the following.

4.2. Numerical simulation of self-similar symmetric α -stable processes

There are two distinct algorithms typically used to generate stationary self-similar S α S-distributed processes characterized by the exponents α and H . One approach utilizes fractional calculus and derives the fractional integral or fractional derivative $X_{\nu,\alpha}(t)$ of an uncorrelated S α S-process $X_\alpha(t)$ in Fourier space, $\hat{X}_\alpha(\omega) = (2\pi)^{-1} \int_{\mathbb{R}} X_\alpha(t') \exp\{-it'\omega\} dt'$, [Chechkin and Gonchar, 2000],

$$\hat{X}_{\nu,\alpha}(\omega) = \frac{\hat{X}_\alpha(\omega)}{(i\omega)^\nu}, \quad \nu = H - 1/\alpha. \quad (11)$$

Hence, this approach is very similar to the established Fourier-filtering technique often used for generating correlated Gaussian noises, see e. g. [Schumann and Kantelhardt, 2011]. Note that Chechkin and Gonchar [2000] restrict their algorithm to $1 \leq \alpha \leq 2$ ³. They further discuss why high-frequency inaccuracies of fractional integration disturb numerical simulations in the anti-persistent case, see also [Chechkin and Gonchar, 2001] for their comprehensive study of fractional Gaussian integration.

The other algorithm is based on discretizing and numerically solving a stochastic integral that defines a *cumulative* self-similar S α S process $Y_{H,\alpha}(t)$, often called fractional Lévy motion,

$$Y_{H,\alpha}(t) = C_{H,\alpha}^{-1} \int_{\mathbb{R}} \left((t-s)_+^{H-1/\alpha} - (-s)_+^{H-1/\alpha} \right) dY_\alpha(s) \quad (12)$$

where $Y_\alpha(s)$ is (standard) S α S motion and $C_{H,\alpha}$ is some norming constant. The increments $X_{H,\alpha}(k) = Y_{H,\alpha}(k) - Y_{H,\alpha}(k-1)$ in the discretized version of Eq. (12) then define a self-similar S α S process $X_{H,\alpha}$ that we study here. Note that the norming constant is chosen such that (i) the S α S scaling parameter is $\gamma = 1$ as previously discussed for deriving Eq. (9) from Eq. (8) and (ii) the probability density functions are equal for the independent and self-similar S α S process. A stochastic integral such as in Eq. (12) can be discretized and efficiently be solved by exploiting the convolution theorem and employing a fast Fourier transform, for further details we refer to [Stoev and Taqqu, 2004]⁴.

In the following, we present results for self-similar S α S processes using the latter algorithm [Stoev and Taqqu, 2004] but we obtain very similar results using the former one [Chechkin and Gonchar, 2000] over the range of its established validity. These processes are parametrized by the two parameters H and α ($\gamma = 1, \delta = \beta = 0$ in Eqs. (8) and (9)). Two further parameters m and M are required by the used algorithm. They control the mesh-size (intermediate points) and the kernel of the fast Fourier transform, respectively. We chose the parameters $m = 64$ and $M = 48576$ and generate time series of length $n = 1000000$. This choice of m and M with $mM \ll n$ is motivated by our observation that an undesired crossover in the scaling behavior of different parameters appears at scales of the order mM ⁵. To the best of our knowledge, this has not been noticed before. Indeed, much shorter time series with $n + M = 2^{14}$, $m_{\max} = 256$, and $M_{\max} = 6000$ were studied by [Stoev and Taqqu, 2004] who concluded that larger values of m should be chosen for $0 < \alpha \leq 1$ while smaller m are preferable for $1 < \alpha \leq 2$ and small M . This is clearly not supported by our simulations for much larger values of n ⁶, which are necessary to estimate extreme value and record statistics of self-similar S α S processes reliably⁷.

For each parameter set (α, H) we generate $N_{\text{conf}} = 1500$ long-range persistent data sets⁸. For surrogate testing we destroy correlations by shuffling those data sets using a Mersenne-Twister-19937 pseudo-random number generator [Matsumoto and Nishimura, 1998] which was also used to generate white Gaussian noise being the basis for the uncorrelated S α S noise⁹.

5. Effects of long-range memory on the statistical properties of symmetric α -stable processes

5.1. Extreme value statistics

Since the theoretical analysis of extreme value statistics is mostly concerned with *asymptotic* distributions as discussed in section 2, these findings are not immediately applicable to time series $\{x_i\}_{i=1,\dots,n}$ of finite length n which are measured in natural systems. In particular, the exact cumulative distribution function $F(x)$ is generally unknown and, hence, neither is $F^n(m)$ in Eq. (1). Thus, one typically has to assume that i) the given time series is a single realization of an underlying stationary stochastic process and ii) the underlying dynamics is ergodic such that one can use time averages instead of or in addition to ensemble averages. This allows one to estimate the distribution of the (block) maximum or extreme value $M_R = \max\{X_1, \dots, X_R\}$ from the given time series by considering non-overlapping blocks of size $R \ll n$. To be more specific, the sequence of maximum values in disjoint blocks of length R is given by $\{m_j\}_{j=1,\dots,[n/R]}$ where $m_j = \max\{x_{(j-1)R+1}, x_{(j-1)R+2}, \dots, x_{jR}\}$ is the maximum in block j and $[\cdot]$ denotes the integer division; see Fig. 2 for an illustration. Under the above assumptions, the estimated distribution $P_R(m)$ of the block maxima should converge towards a specific $G(m)$ as $R \rightarrow \infty$ if a suitable sequence $\{a_n, b_n\}$ exists as in Eq. (2). If this convergence is sufficiently fast, one can estimate $G(m)$ reliably even for finite R (and n) and a finite number of realizations N_{conf} provided that $[n/R] \times N_{\text{conf}} \gg 1$.

For independent symmetric α -stable distributed processes, it is well-known that the asymptotic limit distribution of its extreme values is the Fréchet distribution in Eq. (3b) [Embrechts et al., 1997] since $\bar{P}(x) \sim x^{-1-\alpha}$. More recently, it was proved mathematically that all self-similar S α S processes with $\alpha < 2$ also converge in distribution to the Fréchet extreme value distribution [Samorodnitsky, 2004]. Thus, the presence of long-range memory in the form of persistence or anti-persistence does not have any significant influence on the asymptotic behavior in this case of stationary processes. However, we find that there are significant finite size effects, i.e. significant differences in the extreme value distribution for finite R between the cases with and without long-range memory.

To see this, we estimate the probability density function $P_R(m)$ of the maxima or extreme values in non-overlapping blocks of length R which are shown in Figures 3 and 4 for self-similar S α S processes with different parameters H and α including persistent as well as anti-persistent cases. There are clear differences between the original data and the independent surrogate data, both of which were generated as described in section 4.2. These differences are particularly pronounced for small values of m and R and for strongly persistent cases ($H = 0.9$). For small m , we observe that persistence and anti-persistence lead to different behaviors: the probability of finding a smaller m is enhanced in the case of persistence when compared to the surrogate data, while in the case of anti-persistence the behavior depends sensitively on R . Nevertheless, in the latter case there seems to be a clear and rapid convergence to the distribution of the independent surrogate data with increasing R . Specifically, there are no significant differences for $R > 1000$. This observation can be readily explained. Anti-persistence implies

that in an associated time series large values tend to be followed by small values and small values are rather followed by large values which is similar to an alternating behavior. This alternating behavior does not significantly constrain the maximum value found in a given block if its size is sufficiently large. Thus, long-range memory in the form of anti-persistence does not play an important role for the extreme value distribution even for finite R .

The situation is very different for the case with long-range persistence. Since persistence corresponds to a clustering of large and small values, respectively, more blocks will contain only smaller values such that the block maximum will also be smaller than what would be expected based on independent values. Thus, the distribution of block maxima will indicate a higher probability to find smaller values compared to the independent surrogate data. This is exactly what Figures 3 and 4 show for $H = 0.9$, independent of R . As expected, the deviations from the extreme value distribution of the surrogate data are larger for stronger persistence as a comparison of $\alpha = 1.5$ and $\alpha = 1.8$ shows. Thus, long-range memory in the form of persistence reduces the probability of observing very large block maxima for finite R . This is quantified by Fig. 5, which shows the exceedance probability defined as

$$E_R(m) = \Pr(M_R > m) = \int_m^\infty P_R(m') dm'. \quad (13)$$

This phenomenon is not only true for self-similar S α S processes considered here but also for stationary long-range correlated Gaussian and exponentially distributed processes [Eichner et al., 2006].

In order to test how closely the probability density function $P_R(m)$ of the block maxima for finite R resembles its asymptotic limit given by the generalized extreme value distribution in Eq. (4), we employ a maximum likelihood estimation method – already implemented in Matlab’s Statistics Toolbox – to estimate its parameters and to quantify the goodness-of-fit [Aldrich, 1997; MathWorks Matlab, R2009b]. The values of the shape parameters ξ determining the distribution class are reported for all considered values of H and α in Table 1 in the Appendix. Fig. 6 illustrates the convergence of ξ_R to $1/\alpha$ as $R \rightarrow \infty$ for selected values. The fits themselves are shown in Figures 3 and 4. While there are significant deviations from the GEV distribution for small R and strong persistence, we find relative agreement for $R \geq 10000$ in all cases considered. However, we observe systematic deviations from the theoretical value $1/\alpha$ for very large R . Although errors increase, the systematic underestimation of the shape parameter is possibly not exclusively caused by finite size effects but might be due to short-comings in the GEV fitting algorithm as well as the data generation algorithm.

Further evidence for the rapid convergence to the asymptotic GEV distribution comes from the scaling of the mean, $\langle m \rangle_R$, the median, med_R , and the estimated scale parameter, σ_R , with R (see Eq. (4)), which is shown in Fig. 7. For large R , the scaling approaches the same limit for the self-similar S α S processes and the independent surrogate data¹⁰. For the rescaling coefficient a_R in Eq. (2), it is known that $a_R \propto R^{1/\alpha}$ asymptotically [Embrechts et al., 1997]. This follows from studies of the domain of attraction of the Fréchet class, which have proved that if the cumulative distribution function $F(x)$ of the stochastic process decays asymptotically as $\bar{F}(x) \sim L(x)x^{-\alpha}$, then the rescaling coefficient $a_R = R^{1/\alpha}L(R)$ for some slowly varying function L [Embrechts et al., 1997]. $L(R) \equiv \text{constant}$ for S α S processes. It was also shown that centering is not necessary, i. e., $b_R = 0$ [Embrechts et al., 2004].

Nevertheless, there exist to our best knowledge no analytical derivations on the convergence of $\langle m \rangle_R$, med_R , and σ_R . We expect a similar behavior in the limit $R \rightarrow \infty$ where

a unique Fréchet distribution is approached. While we observe a scaling similar to a_R for the median in Fig. 7(b) and with reservations for the scale σ_R in Fig. 7(c) there are still noticeable deviations for the mean $\langle m \rangle_R$, and for that reason we exclusively focus on medians in our discussion of conditional extremes, see Sect. 5.2. Besides this, Fig. 7 provides further evidence that the asymptotic scaling of the renormalization sequence $\{a_n, b_n\}$ — which ensures the convergence in Eq. (2) — is not affected by the presence of long-range memory. Yet, we also see clear deviations from the asymptotic scaling for small R as expected. In particular, we observe a crossover in the medians at scales somewhat below $R_\times = 100$ for $\alpha = 1.5$ and around $R_\times = 600 - 700$ for $\alpha = 1.8$ in the medians. Note that this crossover is apparently independent of H . This indicates that long-range memory does not play a role for the deviations from the asymptotic scaling. Instead, the ‘heavier’ the heavy-tailed distribution, the smaller R_\times .

Based on the observed scaling behavior, it is straightforward to identify a suitable sequence $\{a_R, b_R\}$ to ensure that Eq. (2) holds. Namely, we chose

$$a_R = R^{1/\alpha} \text{ and } b_R = 0. \quad (14)$$

Using this sequence, we can rescale the probability density functions in Figs. 3 and 4 according to Eq. (2) in order to obtain a scaling collapse resembling the asymptotic distribution. This is shown in Figs. 8 and 9. While the collapse in the tails is excellent in all considered cases, the collapse is often not as good for small arguments. This is particularly true for large α and large H and confirms the findings above.

5.2. Conditional extrema and hazard assessment

As a consequence of long-range memory in self-similar S α S processes, the value of $X(t)$ for a given t depends on the values at all earlier times. Thus, the probability of finding a certain value m_{j+1} as the block maximum also depends on the history and, thus, the preceding block maxima m_k with $k \leq j$. This directly allows one to make a time-dependent hazard assessment and potentially even predict the size of future extreme values based on the history of block maxima. In the absence of memory as for the iid case, only time-independent hazard assessment is possible.

As one possible approach to time-dependent hazard assessment, we study the statistics of all block maxima m_{j+1} in the sequence of maxima $\{m_j\}_{j=1, \dots, [N/R]}$ that follow a block maximum $m_j = m_0$ within a certain range — see [Schweiger and Davidsen, 2011] for a related but different approach. For example, Figs. 10(a,b) display the conditional probability density functions of block maxima m that follow a block maximum m_0 larger or equal than a threshold. The thresholds were chosen to obtain 15000 conditional maxima when combining all realizations¹¹. As can be seen, long-range persistence shifts the distributions to the right compared to the independent surrogate case. The latter is equivalent to the iid case. Note that the results for the inverse condition (m_0 is smaller than the threshold) are also indistinguishable from the iid case. Panels (c,d) report the corresponding exceedance probabilities, clearly indicating clustering of extremes in the presence of long-range persistence compared with the time-independent case, i. e., larger events are more likely followed by large events in the time-dependent case.

For a more complete understanding we now define the conditions m_0 as the geometric averages of non-overlapping and exponentially growing ranges and combine bins at both ends to ensure at least 1000 conditional maxima per bin¹². Figures 11 and 12 report the full results for conditional medians $med_R(m_{k,0}) = \text{median}\{m_{j,2, \dots, n} | m_{j-1} = m_{k,0}\}$ where

the conditions $m_{k,0}$ are understood as ranges defined by the k -th bin. In addition to the conditional median of self-similar SaaS distributed time series we also show the conditional medians for the randomized sequence of block maxima for comparison. Shuffling the raw data affects the distribution of block maxima depending on the block size R . Hence, for generating independent surrogates it is here important to shuffle the sequence of block maxima and *not* the underlying time series $\{x_i\}_i$ to preserve the distribution of block maxima. Note that shuffling the block maxima is equivalent to destroying long-range memory in $\{x_i\}$ on scales larger than the block size but preserving memory on smaller scales [Schumann and Kantelhardt, 2011]. Considering the surrogates corresponds to a time-independent hazard assessment. We observe that $med_R(m_0)$ increases monotonically with m_0 in the case of strong persistence, again a clear indication of the clustering of block maxima. This dependence becomes less pronounced for larger R and indeed it should vanish in the limit $R \rightarrow \infty$. This is also true for other processes with long-range persistence [Eichner et al., 2006]. In the case of anti-persistence, the deviations from the expected behavior for independent maxima are much smaller and only significant for small R . As expected, the behavior is opposite to the case of persistence: $med_R(m_0)$ decreases monotonically with m_0 .

5.3. Record Statistics

While the theoretical results for record statistics presented in section 3 are all based on the assumption of iid processes, not much is known about the case of stationary processes with long-range memory [Newman et al., 2010]. For self-similar SaaS processes, we first analyze the probability $P(N_R)$ to find N_R records given a sequence of length R . As Fig. 13 shows for $R = 10000$, this probability only deviates significantly from the iid prediction — which is independent of the underlying distribution as follows from the discussion in section 3 — in the case of strong persistence ($H > 1/\alpha$). Since persistence implies that large values tend to follow large values and small values rather follow small values, one expects that there is higher probability to encounter a small number of records as well a larger number of records compared to the iid prediction. This is exactly what Fig. 13 shows. While the above results could be specific to the chosen R , this is not confirmed by the dependence of the mean number of records $E(N_t)$ on t with $t \leq R$. Indeed, Fig. 14 indicates that strong deviations from the iid behavior described by Eq. (6a) only occur in the presence of strong persistence. While the influence of persistence on record statistics is easily detectable in $E(N_t)$ and $P(N_R)$, the effect is more subtle if one considers the probability to break a record at a time t , $P(X_t = \max\{x_1, \dots, x_t\})$, see Fig. 14. This is related to the fact, that the former are cumulative measures of the later as follows directly from the discussion in section 3.

Our results are consistent with earlier numerical findings for stationary Gaussian processes with persistent long-range memory [Newman et al., 2010]. The authors found that the expected number of records $E(N_t)$ for fixed t increased monotonically with increasing persistence.

6. Application: Solar power input into the Earth's magnetosphere

The solar wind is a prime example of plasma turbulence at low frequency magnetohydrodynamic scales as evident from its power-law energy distribution [Zhou et al., 2004], the magnetic field correlations [Matthaeus et al., 2005] and its intermittent dynamics [Burlaga, 2001]. While understanding this type of turbulence is an important challenge by itself, understanding the interplay between the solar wind and the

Earth's magnetosphere is another open problem of considerable interest [Baker, 2000]. The difficulty of understanding the magnetospheric response to the solar wind variations is intimately related to the observed range of mechanisms of energy release and multiscale coupling phenomena [Angelopoulos et al., 1999; Lui et al., 2000; Uritsky et al., 2002; Borovsky and Funsten, 2003; D'Amicis et al., 2007; Uritsky et al., 1998; Chang, 1999; Chapman et al., 1999; Klimas et al., 2000; Sitnov et al., 2001; Consolini, 2002; Aschwanen, 2011]. Here, we focus on the Akasofu ϵ parameter which is a solar-wind proxy for the energy input into the Earth's magnetosphere (see [Koskinen and Tanskanen, 2002] for a more recent discussion). In SI units it is defined as

$$\epsilon = v \frac{B^2}{\mu_0} \ell_0^2 \sin^4(\theta/2), \quad (15)$$

where v is the solar wind velocity, B is the magnetic field, $\mu_0 = 4\pi \times 10^{-7}$ is the permeability of free space, $\ell_0 \approx 7R_E$, and $\theta = \arctan(|B_y|/B_z)$. Geocentric solar magnetospheric (GSM) coordinates are used.

The ACE spacecraft [Stone et al., 1998] orbits the Earth-Sun L1 libration point approximately 1.5×10^9 m from the Earth and monitors solar wind, interplanetary magnetic fields and high energy particles. The data can be downloaded from <http://cdaweb.gsfc.nasa.gov>. Specifically, for the years 2000-2007, we extracted the magnitude of the x -component of the solar wind, and the y and z components of the magnetic fields, as seen respectively by the SWEPAM and MAG instruments (level 2 72 data) of the ACE spacecraft, all in GSM coordinates. The choice of components reflect the Poynting flux interpretation of the ϵ parameter. For the most part, measurements are available every 64 and 16s for the wind velocity and magnetic fields, respectively. We calculated the ϵ parameter given by Eq. (15) every 64s. Since the wind velocity and magnetic field measurements are not synchronized, we linearly interpolated the magnetic field measurements towards the time of the nearest wind velocity measurement. For these 8 years the ϵ time series consisted of 3 944 700 points; see Fig. 15(a). Measurements for wind velocities or magnetic fields are sometimes unavailable. Approximately 9 per cent of the points comprising the ϵ series are missing. As in [Moloney and Davidsen, 2011], we set missing data points to the value of the last valid recording proceeding them (irrespective of the size of the data gap), thereby creating plateaus of constant intensity. This minimises artifacts associated with points missing at regular experiment-specific frequencies. We have checked that nothing changes crucially in our statistical analyses by adopting other schemes.

Watkins et al. [2005] have suggested to model the ϵ parameter by a fractional Lévy motion as defined by Eq. (12), which implies that the series of changes in ϵ , $\Delta_\tau \epsilon(t_k) = \epsilon(t_k + \tau) - \epsilon(t_k)$ with $t_k = t_0 + k\tau$ for $k \geq 0$, should form a self-similar SaaS process. For the ϵ time series studied here and shown in Fig. 15(b) for $\tau = 64$ s, Moloney and Davidsen [2010] have found that the properties of self-similarity and α -stability both roughly hold for $64s \leq \tau \leq 4$ h. Specifically, they found $\alpha = 1.55$ and $H = 0.40$ indicating the presence of weak anti-persistence. Similar values have been observed for other ϵ series (see [Moloney and Davidsen, 2010] and references therein) always indicting the presence of anti-persistence. Given these properties, one might ask to which extent the numerical results for time-dependent hazard assessment and records statistics of self-similar SaaS processes presented in Section 5 apply to the $\Delta_\tau \epsilon$ series. This will be addressed in the following.

6.1. Conditional extrema and hazard assessment

Fig. 16 shows that the median of the conditional distribution of the block maxima, $\text{med}_R(m_0)$, increases monotonically and approximately as a power law with m_0 for $\tau = 64\text{s}$. As τ is increased the power law's exponent decreases, eventually leaving the power law regime, and approaching the iid case (median independent of condition) in the limit of very large τ . Note that the median values of the block maxima and their corresponding surrogates, obtained by shuffling the block maxima, naturally increase for larger block sizes since the fewer blocks are more and more dominated by the largest extreme values in the time series (cp. $\tau = 8192\text{s}$). Our findings indicate clustering of extreme values for not too large τ and, thus, persistence — in sharp contrast to what is expected for anti-persistent self-similar S α S processes (see Figs. 11, 12). This contradiction provides clear evidence that only some properties of the $\Delta_\tau\epsilon$ series can be (roughly) characterized by a self-similar S α S process. In particular, the memory reflected in the $\Delta_\tau\epsilon$ is not reliably captured by a self-similar S α S process — potentially due to non-stationarities. A similar conclusion has been reached by *Moloney and Davidsen* [2010] who investigated the distributions of block maxima of $\Delta_\tau\epsilon$. Nevertheless, the findings summarized by Fig. 16 show unambiguously that time-dependent hazard assessment can be successfully applied to the considered time series and clearly outperforms any time-independent hazard assessment of future extreme values.

6.2. Record Statistics

The observed clustering in the $\Delta_\tau\epsilon$ series discussed in section 6.1 is also present in the record statistics. Fig. 17 shows that the probability $P(N_R)$ to find N_R records in a sequence of length R is much higher for large N_R than what is expected for the iid case. This is further confirmed by Fig. 18 which shows that the expected number of records grows much faster than in the iid case. Both figures also suggest a dependence on τ . In particular, the deviations from the iid case for large times increase monotonically with τ until they reach a maximum around $\tau = 1024\text{s}$. As τ is increased further the deviations decrease monotonically with τ and finally they approach the iid case in the limit of very large τ . This is supported by the probability to observe a record at an elapsed time t shown in Fig. 19. Note that in contrast to these results found for records the conditional maxima in Fig. 16 apparently showed a monotonic dependence on τ .

6.3. Discussion

While we have focused here on $\Delta_\tau\epsilon$ series, our results with respect to time-dependent hazard assessment are directly applicable to the ϵ series itself. As Fig. 20 shows, there is a strong correlation between $\Delta_\tau\epsilon(t_k)$ and $\epsilon(t_k + \tau)$ — as measured by the Pearson correlation coefficient — if one considers the largest values in $\Delta_\tau\epsilon(t_k)$. This implies that a large extreme value in $\Delta_\tau\epsilon$ typically indicates a large value in ϵ , while a smaller extreme value in $\Delta_\tau\epsilon$ tends to correspond to a smaller value in ϵ — independent of the exact value of τ . Thus, one can translate our findings from Section 6.1: Extreme values in ϵ tend to be clustered, which makes time-dependent hazard assessment in the context of space weather feasible. These results are just a first step and clearly need to be investigated in more detail in future work.

7. Summary

In summary, our numerical analysis of self-similar symmetric α -stable processes has shown that the presence of

long-range memory can lead to significant finite size effects in extreme value and record statistics despite the fact that some of the asymptotic behavior is not affected. The finite size effects are particularly pronounced if the long-range memory leads to persistent behavior. We also found that long-range memory allows a time-dependent hazard assessment of the size of future extreme events based on extreme events observed in the past. Time-dependent hazard assessment based on the value of the previous block maximum significantly outperforms time-independent hazard assessment and, thus, provides a significant improvement.

Moreover, we showed that such a time-dependent hazard assessment is directly applicable in the context of the solar power influx into the magnetosphere. Since many processes in nature are characterized by long-range memory and heavy-tailed distributions — especially in space physics [*Watkins et al.*, 2005; *Moloney and Davidsen*, 2010] — our findings are of general interest. Further examples outside geophysics include communications traffic [*Laskin et al.*, 2002].

Appendix

Acknowledgments. We thank A. Rasmussen for helpful discussions. This project was supported by Alberta Innovates (formerly Alberta Ingenuity).

Notes

1. Since $\min\{X_1, \dots, X_n\} = \max\{-X_1, \dots, -X_n\}$, the minimum can be mathematically treated in the same way.
2. Similarly, one can define a lower record $X_m = \min\{X_1, \dots, X_m\}$.
3. This limitation mainly comes from the loss of validity of the Minkowski inequality for $\alpha < 1$, which is used in [*Chechkin and Gonchar*, 2000] to estimate the upper boundary of H . It should nevertheless be possible to generalize the algorithm to arbitrary $\alpha \in (0, 2]$. Moreover, one possible pitfall of the algorithm is that the probability density of the generated self-similar S α S process is not explicitly renormalized to be the same as for the uncorrelated noise it is initialized with. This has to be done manually.
4. A similar supposedly faster algorithm was suggested later [*Wu et al.*, 2004], but not tested by us.
5. This crossover is not present in the algorithm by *Chechkin and Gonchar* [2000].
6. We also noted a number of artifacts in the generated time series for values $\alpha < 1$ which we do not consider in this paper. One might be able to resolve these artifacts by significantly increasing the mesh size parameter m . However, doubling m results in practically doubling the memory requirements unless the series length n is reduced accordingly. We plan on testing this more systematically in the future.
7. Note further that the values were chosen to ensure that $m(M + n)$ is an integer power of 2.
8. Note that significant computational resources are required. For a single parameter set (α, H) , about 15GB are necessary to store the ‘double’ raw data. Since the computation of the involved Fourier transform requires to allocate arrays of size $m(M + n)$ and there is a noticeable overhead for computation, main memory requirements become an issue very quickly as m and M grow.
9. Uncorrelated S α S distributed random numbers can be generated from uncorrelated Gaussian distributed random numbers following [*Chambers et al.*, 1976, 1987].
10. Note that the differences between the different surrogate data are partly statistical and partly due to the algorithm discussed in section 4.2.
11. This corresponds to the upper 0.999-quantile, or 1 per mille of all maxima.

Table 1. Shape parameters ξ and corresponding maximum error obtained from 95%-confidence intervals of a maximum likelihood fit of Eq. (4) to the data. Note that for $R \leq 100$ there was often no convergence in the estimation meaning the probability density cannot be properly approximated by the GEV distribution in Eq. (4). Positive values of ξ indicate a Fréchet distribution. Asymptotically, ξ should approach $1/\alpha$ based on theoretical results [Samorodnitsky, 2004].

	$\alpha = 1.5$		$\alpha = 1.8$	
	self-similar S α S shape ξ	shuffled S α S shape ξ	self-similar S α S shape ξ	shuffled S α S shape ξ
H=0.1 R=1000 R=10000	0.6679 ± 0.0017 0.6582 ± 0.0054	0.6657 ± 0.0017 0.6532 ± 0.0054	0.5751 ± 0.0017 0.5489 ± 0.0051	0.5734 ± 0.0017 0.5448 ± 0.0050
H=0.2 R=1000 R=10000	0.6682 ± 0.0017 0.6575 ± 0.0054	0.6653 ± 0.0017 0.6510 ± 0.0054	0.5756 ± 0.0017 0.5491 ± 0.0051	0.5738 ± 0.0017 0.5443 ± 0.0050
H=0.3 R=1000 R=10000	0.6682 ± 0.0017 0.6573 ± 0.0054	0.6647 ± 0.0017 0.6509 ± 0.0054	0.5763 ± 0.0017 0.5498 ± 0.0051	0.5738 ± 0.0017 0.5451 ± 0.0051
H=0.4 R=1000 R=10000	0.6683 ± 0.0017 0.6584 ± 0.0054	0.6649 ± 0.0017 0.6501 ± 0.0054	0.5764 ± 0.0017 0.5501 ± 0.0051	0.5739 ± 0.0017 0.5473 ± 0.0051
H=0.5 R=1000 R=10000	0.6685 ± 0.0017 0.6589 ± 0.0054	0.6654 ± 0.0017 0.6513 ± 0.0054	0.5761 ± 0.0017 0.5515 ± 0.0051	0.5756 ± 0.0016 0.5496 ± 0.0051
H=0.6 R=1000 R=10000	0.6684 ± 0.0017 0.6608 ± 0.0054	0.6667 ± 0.0017 0.6556 ± 0.0054	0.5751 ± 0.0017 0.5533 ± 0.0051	0.5756 ± 0.0017 0.5488 ± 0.0051
H=0.7 R=1000 R=10000	0.6681 ± 0.0017 0.6625 ± 0.0054	0.6675 ± 0.0017 0.6568 ± 0.0054	0.5742 ± 0.0016 0.5530 ± 0.0051	0.5714 ± 0.0017 0.5418 ± 0.0051
H=0.8 R=1000 R=10000	0.6656 ± 0.0017 0.6622 ± 0.0054	0.6586 ± 0.0017 0.6431 ± 0.0054	0.5496 ± 0.0011 0.5519 ± 0.0051	0.5653 ± 0.0017 0.5296 ± 0.0051
H=0.9 R=1000 R=10000	0.4199 ± 0.0017 0.6613 ± 0.0054	0.6410 ± 0.0006 0.6202 ± 0.0054	0.2716 ± 0.0005 0.5484 ± 0.0051	0.5510 ± 0.0017 0.5108 ± 0.0050

12. We start with a set of $N_{\text{bin}} = 20$ non-overlapping logarithmic bins, $\{\mathfrak{M}_k\}_{k=1,\dots,N_{\text{bin}}} = \{[m_{k,\text{min}}, m_{k,\text{max}}]\}_k$ with $m_{k,\text{min}} \leq m_{k,\text{max}}$ and $m_{1,\text{min}} > 0$, and associate the geometric mean $m_{k,0} = (m_{k,\text{min}} m_{k,\text{max}})^{1/2}$ with the condition $m_{k,0}$. Due to the heavy tails in the Fréchet distribution, outer bins are much less populated than bins in the center. We therefore combine bins on both edges, starting from $k = 1$ and $k = N_{\text{bin}}$ and proceeding towards the center, until at least 1000 maxima m_j are contributing to each bin.

References

- Albeverio, S., V. Jentsch, and H. Kantz (Eds.), *Extreme events in nature and society*, Springer, 2006.
- Aldrich, J., R. A. Fisher and the making of maximum likelihood 1912-1922, *Statistical Science*, 12(3), 162–176, doi: 10.1214/ss/1030037906, 1997.
- Angelopoulos, V., T. Mukai, and S. Kokubun, Evidence for intermittency in Earth's plasma sheet and implications for self-organized criticality, *Physics of Plasmas*, 6, 4161, 1999.
- Aschwanden, M., *Self-organized criticality in astrophysics*, Springer, 2011.
- Baker, D. N., Effects of the sun on the earth's environment, *Journal of Atmospheric and Solar-Terrestrial Physics*, 62(17-18), 1669, 2000.
- Benestad, R. E., How often can we expect a record event?, *Climate Research*, 25, 3, 2003.
- Benestad, R. E., A simple test for changes in statistical distributions, *EOS, Transactions, American Geophysical Union*, 89, 389, 2008.
- Berman, S. M., Limit theorems for the maximum term in stationary sequences, *The Annals of Mathematical Statistics*, 33, 502, 1964.
- Bogachev, M. I., J. F. Eichner, and A. Bunde, Effect of nonlinear correlations on the statistics of return intervals in multifractal data sets, *Physical Review Letters*, 99, 240601, 2007.
- Borovsky, J. E., and H. O. Funsten, Role of solar wind turbulence in the coupling of the solar wind to the Earth's magnetosphere, *Journal of Geophysical Research*, 108(A6), 1246, 2003.
- Bruno, R., L. Sorriso-Valvo, V. Carbone, and B. Bavassano, A possible truncated-Lévy-flight statistics recovered from interplanetary solar-wind velocity and magnetic-field fluctuations, *Europhysics Letters*, 66(1), 146, 2004.
- Bunde, A., J. Kropp, and H. J. Schellnhuber (Eds.), *The science of disasters: Climate disruptions, heart attacks and market crashes*, Springer, 2002.
- Burlaga, L. F., Lognormal and multifractal distributions of the heliospheric magnetic field, *Journal of Geophysical Research*, 106(A8), 15917, 2001.
- Caers, J., J. Beirlant, and M. A. Maes, Statistics for modeling heavy tailed distributions in geology : Part II. applications, *Mathematical Geology*, 31(4), 1999.
- Chambers, J. M., C. L. Mallows, and B. W. Stuck, A Method for Simulating Stable Random Variables, *Journal of the American Statistical Association*, 71(354), 340, 1976.
- Chambers, J. M., C. L. Mallows, and B. W. Stuck, Corrections : A Method for Simulating Stable Random Variables, *Journal of the American Statistical Association*, 82(398), 704, 1987.
- Chandler, K. N., The Distribution and Frequency of Record Values, *Journal of the Royal Statistical Society. Series B (Methodological)*, 14(2), 220, 1952.
- Chang, T., Self-organized criticality, multi-fractal spectra, sporadic localized reconnections and intermittent turbulence in the magnetotail, *Physics of Plasmas*, 6(11), 4137, 1999.
- Chapman, S. C., R. O. Dendy, and G. Rowlands, A Sandpile Model with Dual Scaling Regimes for Laboratory, Space, and Astrophysical Plasmas, *Physics of Plasmas*, 6(11), 4169, (1999).
- Chechkin, A., and V. Gonchar, A model for persistent Lévy motion, *Physica A*, 277(3–4), 312, 2000.
- Chechkin, A., and V. Gonchar, Fractional Brownian motion approximation based on fractional integration of a white noise, *Chaos, Solitons & Fractals*, 12(2), 391, doi:10.1016/S0960-0779(99)00183-6, 2001.
- Coles, S., *An Introduction to Statistical Modeling of Extreme Values*, Springer Series in Statistics, 4 ed., Springer, 2007.
- Consolini, G., Self-Organized Criticality: A new paradigm for the magnetotail dynamics, *Fractals*, 10(3), 275, 2002.
- D'Amicis, R., R. Bruno, and B. Bavassano, Is the geomagnetic activity driven by solar wind turbulence?, *Geophysical Research Letters*, 34, L05108, 2007.
- Davidson, J., P. Grassberger, and M. Paczuski, Earthquake recurrence as a record breaking process, *Geophysical Research Letters*, 33(11), L11304, doi:10.1029/2006GL026122, 2006.
- Davidson, J., P. Grassberger, and M. Paczuski, Networks of recurrent events, a theory of records, and an application to finding causal signatures in seismicity, *Physical Review E*, 77(6), 066104, doi:10.1103/PhysRevE.77.066104, 2008.
- de Haan, L., and A. Ferreira, *Extreme Value Theory: An Introduction*, Springer Series in Operations Research and Financial Engineering, Springer, 2006.
- Easterling, D. R., G. A. Meehl, C. Parmesan, S. A. Changnon, T. R. Karl, and L. O. Mearns, Climate extremes: Observations, modeling, and impacts, *Science*, 289, 2968, 2000.
- Efron, B., 1977 Rietz Lecture - bootstrap methods - another look at the jackknife, *Annals of Statistics*, 7(1), 1, 1979.
- Efron, B., and R. J. Tibshirani, *An Introduction to the Bootstrap*, Chapman & Hall, 1993.
- Eichner, J. F., J. W. Kantelhardt, A. Bunde, and S. Havlin, Extreme value statistics in records with long-term persistence, *Physical Review E*, 73, 016130, 2006.
- Embrechts, P., and M. Makoto, *Selfsimilar Processes*, Princeton Series in Applied Mathematics, Princeton University Press, 2002.
- Embrechts, P., and H. Schmidli, Modelling of extremal events in insurance and finance, *ZOR - Mathematical Methods of Operations Research*, 39(1), 1, doi:10.1007/BF01440733, 1994.
- Embrechts, P., T. Mikosch, and C. Klüppelberg, *Modelling Extremal Events, Applications of Mathematics. Stochastic Modelling and Applied Probability*, vol. 33, 4 ed., Springer, 1997.
- Embrechts, P., C. Klüppelberg, and T. Mikosch, *Modelling extremal events for insurance and finance*, Springer, Berlin, 2004.
- Galambos, J., J. Lechner, and E. Simin (Eds.), *Extreme value theory and applications*, Kluwer, Dordrecht, 1994.
- Glaser, R., and H. Stangl, Climate and floods in central Europe since AD 1000: data, methods, results and consequences, *Surveys in Geophysics*, 25, 485, 2004.
- Glick, N., Breaking records and breaking boards, *The American Mathematical Monthly*, 85(1), 2, 1978.
- Györgyi, G., N. R. Moloney, K. Ozogány, and Z. Rácz, Finite-size scaling in extreme statistics, *Physical Review Letters*, 100, 210601, 2008.
- Hnat, B., S. C. Chapman, and G. Rowlands, Intermittency, scaling, and the Fokker-Planck approach to fluctuations of the solar wind bulk plasma parameters as seen by the WIND spacecraft, *Physical Review E*, 67(5), 056404, 2003.
- Hurst, H. E., Long-term storage capacity of reservoirs, *Transaction of the American Society of Civil Engineers*, 116, 770, 1951.
- Huybers, P., and W. Curry, Links between annual, Milankovitch, and continuum temperature variability, *Nature (London)*, 441, 329, 2006.
- Kantelhardt, J. W., D. Rybski, S. A. Zschiegner, P. Braun, E. Koscielny-Bunde, V. Livina, S. Havlin, and A. Bunde, Multifractality of river runoff and precipitation: comparison of fluctuation analysis and wavelet methods, *Physica A*, 330, 240, 2003.
- Kantelhardt, J. W., E. Koscielny-Bunde, D. Rybski, P. Braun, A. Bunde, and S. Havlin, Long-term persistence and multifractality of precipitation and river runoff records, *Journal of Geophysical Research, Atmospheres*, 111(D1), doi: 10.1029/2005JD005881, 2006.
- Klimas, A. J., J. A. Valdivia, D. V. Vassiliadis, D. N. Baker, M. Hesse, and J. Takalo, Self-organized criticality in the substorm phenomenon and its relation to localized reconnection in the magnetospheric plasma sheet, *Journal of Geophysical Research*, 105(A8), 18765, 2000.
- Koscielny-Bunde, E., H. Roman, A. Bunde, S. Havlin, and H. Schellnhuber, Long-range power-law correlations in local daily temperature fluctuations, *Philosophical Magazin B Physics of Condensed Matter*, 77(5), 1331, 1998.

- Koskinen, H. E. J., and E. I. Tanskanen, Magnetospheric energy budget and the epsilon parameter, *Journal of Geophysical Research*, 107, 42, 2002.
- Laskin, N., I. Lambadaris, F. C. Harmantzis, and M. Devetsikiotis, Fractional Lévy motion and its application to network traffic modeling, *Computer Networks*, 40, 363, 2002.
- Leadbetter, M. R., and H. Rootzén, Extremal theory for stochastic processes, *Annals of Probability*, 16, 431, 1988.
- Leadbetter, M. R., G. Lindgren, and H. Rootzen, *Extremes and related properties of random sequences and processes*, Springer, New York, 1983.
- Lui, A. T. Y., S. C. Chapman, K. Liou, P. T. Newell, C. I. Meng, M. Brittacher, and G. K. Parks, Is the dynamimc magnetosphere an avalanching system?, *Geophysical Research Letters*, 27, 911, 2000.
- MathWorks Matlab, Statistics toolbox, Software Package, R2009b.
- Matsumoto, M., and T. Nishimura, Mersenne twister: a 623-dimensionally equidistributed uniform pseudo-random number generator, *ACM Transactions on Modeling and Computer Simulation (TOMACS) - Special issue on uniform random number generation*, 8(1), 3, 1998.
- Matthaeus, W. H., S. Dasso, J. M. Weygand, L. J. Milano, C. W. Smith, and M. G. Kivelson, Spatial correlations of solar-wind turbulence from two-point measurements, *Physical Review Letters*, 95, 231101, 2005.
- Moloney, N. R., and J. Davidsen, Extreme value statistics and return intervals in long-range correlated uniform deviates, *Physical Review E*, 79, 041131, 2009.
- Moloney, N. R., and J. Davidsen, Extreme value statistics in the solar wind: An application to correlated Lévy processes, *Journal of Geophysical Research*, 115(A10), doi:10.1029/2009JA015114, 2010.
- Moloney, N. R., and J. Davidsen, Extreme bursts in the solar wind, *Geophysical Research Letters*, 38, L14111, 2011.
- Monetti, R. A., S. Havlin, and A. Bunde, Longterm persistence in the sea surface temperature fluctuations, *Physica A*, 320, 581, 2002.
- Nevzorov, V. B., *Records: Mathematical Theory, Translations of Mathematical Monographs*, vol. 194, 170 pp., American Mathematical Society, 2001.
- Newman, W. I., B. D. Malamud, and D. L. Turcotte, Statistical properties of record-breaking temperatures, *Physical Review E*, 82(6), 066111, doi:10.1103/PhysRevE.82.066111, 2010.
- Painter, S., and L. Paterson, Fractional Lévy motion as a model for spatial variability in sedimentary-rock, *Geophysical Research Letters*, 21, 2857, 1994.
- Peixoto, T. P., K. Doblhoff-Dier, and J. Davidsen, Spatiotemporal correlations of aftershock sequences, *Journal of Geophysical Research*, 115, B10309, doi:10.1029/2010JB007626, 2010.
- Pelletier, J., and D. L. Turcotte, Long-range persistence in climatological and hydrological time series: analysis, modeling and application to drought hazard assessment, *Journal of Hydrology*, 203, 198, 1997.
- Pommois, P., G. Zimbardo, and P. Veltri, Magnetic field line transport in three dimensional turbulence: Lévy random walk and spectrum models, *Physics of Plasmas*, 5(5), 1288, 1998.
- Redner, S., and M. R. Petersen, Role of global warming on the statistics of record-breaking temperatures, *Physical Review E*, 74(6), 061114, doi:10.1103/PhysRevE.74.061114, 2006.
- Rény, A., Theory des éléments saillants d'une suite d'observations, with summary in english, *Colloquium on Combinatorial Methods in Probability Theory, Matematisk Institut, Aarhus Universitet, Denmark*, pp. 104–117, 1962.
- Roman, H. E., A. Celi, and G. De Filippi, Fluctuation analysis of meteo-marine data, *European Physical Journal - Special Topics*, 161, 195, doi:10.1140/epjst/e2008-00761-4, 2008.
- Samorodnitsky, G., Extreme value theory, ergodic theory and the boundary between short memory and long memory for stationary stable processes, *Annals of Probability*, 32, 1438, 2004.
- Samorodnitsky, G., and M. S. Taqqu, *Stable Non-Gaussian Random Processes: Stochastic Models with Infinite Variance*, Chapman and Hall, 1994.
- Schmittmann, B., and R. K. P. Zia, "Weather" records: musings on cold days after a long hot Indian summer, *American Journal of Physics*, 67, 1269, 1999.
- Schumann, A. Y., *Fluctuations and Synchronization in Complex Physiological Systems*, Logos Verlag, Berlin, 2011.
- Schumann, A. Y., and J. W. Kantelhardt, Multifractal moving average analysis and test of multifractal model with tuned correlations, *Physica A*, 390(14), 2637, 2011.
- Schweiger, T., and J. Davidsen, Clustering of extreme and recurrent events in deterministic chaotic systems, *Physical Review E*, 84, 016202, 2011.
- Sibani, P., and H. J. Jensen, Record statistics and dynamics, in *Encyclopedia of Complexity and System Science*, edited by R. A. Meyers, Springer, New York, 2009.
- Sitnov, M. I., A. S. Sharma, K. Papadopoulos, and D. Vassiliadis, Modeling substorm dynamics of the magnetosphere: From self-organization and self-organized criticality to nonequilibrium phase transitions, *Physical Review E*, 65, 016116, 2001.
- Sornette, D., *Critical Phenomena in Natural Sciences*, 2nd ed., Springer Verlag, Berlin, Germany, 2006.
- Stoev, S., and M. S. Taqqu, Simulation methods for linear fractional stable motion and farima using the fast fourier transform, *Fractals*, 12(1), 95, 2004.
- Stone, E. C., A. M. Frandsen, R. A. Mewaldt, E. R. Christian, D. Margolies, J. F. Ormes, and F. Snow, The advanced composition explorer, *Space Science Reviews*, 86, 1, 1998.
- Taqqu, M. S., Random processes with long-range dependence and high variability, *Journal of Geophysical Research*, 92, 9683, 1987.
- Uritsky, V. I., and M. I. Pudovkin, Low-frequency 1/f-like fluctuations of the AE index as a possible manifestation of self-organized criticality in the magnetosphere, *Annales Geophysicae*, 16, 1580, 1998.
- Uritsky, V. M., A. J. Klimas, D. Vassiliadis, D. Chua, and G. Parks, Scale-free statistics of spatiotemporal auroral emissions as depicted by POLAR UVI images: dynamic magnetosphere is an avalanching system, *Journal of Geophysical Research*, 107(A12), 1426, 2002.
- Van Aalsburg, J., W. I. Newman, D. L. Turcotte, and J. B. Rundle, Record-breaking earthquakes, *Bulletin of the Seismological Society of America*, 100(4), 1800, doi:10.1785/0120090015, 2010.
- van den Brink, H. W., and G. P. Können, The staistical distribution of meteorological outliers, *Geophysical Research Letters*, 35(23), L23702, 2008.
- Vasudevan, K., D. W. Eaton, and J. Davidsen, Intraplate seismicity in canada: a graph theoretic approach to data analysis and interpretation, *Nonlinear Processes in Geophysics*, 17, 513, 2010.
- Vogel, R. M., A. Zafirakou-Koulouris, and N. Matalas, The frequency of record breaking floods in the United States, *Water Resources Research*, 37, 1723, 2001.
- Watkins, N. W., D. Credgington, B. Hnat, S. C. Chapman, M. P. Freeman, and J. Greenhough, Towards synthesis of solar wind and geomagnetic scaling exponents: a fractional Lévy motion model, *Space Science Reviews*, 121, 271, 2005.
- Watkins, N. W., D. Credgington, R. Sanchez, S. J. Rosenberg, and S. C. Chapman, Kinetic equation of linear fractional stable motion and applications to modeling the scaling of intermittent bursts, *Physical Review E*, 79(4), 041124, doi:10.1103/PhysRevE.79.041124, 2009.
- Wergen, G., and J. Krug, Record-breaking temperatures reveal a warming climate, *Europhysics Letters*, 92, 30008, 2010.
- Wu, W., G. Michailidis, and D. Zhang, Simulating sample paths of linear fractional stable motion, *IEEE Transactions on Information Theory*, 50(6), 1086, doi:10.1109/TIT.2004.828059, 2004.
- Zaslavsky, G. M., P. N. Guzdar, M. Edelman, M. I. Sitnov, and A. S. Sharma, Multiscale behavior and fractional kinetics from the data of solar wind-magnetosphere coupling, *Communications in Nonlinear Science and Numerical Simulation*, 13, 314, 2008.
- Zhou, Y., W. H. Matthaeus, and P. Dmitruk, Magnetohydrodynamic turbulence and time scales in astrophysical and space plasmas, *Review of Modern Physics*, 76, 1015, 2004.

A. Y. Schumann, Complexity Science Group, Department of Physics and Astronomy, University of Calgary, 2500 University Dr. NW, Calgary, Alberta T2N 1N4, Canada. (ay.schumann@ucalgary.ca)

J. Davidsen, Complexity Science Group, Department of Physics and Astronomy, University of Calgary, 2500 University Dr. NW, Calgary, Alberta T2N 1N4, Canada. (david-sen@phas.ucalgary.ca)

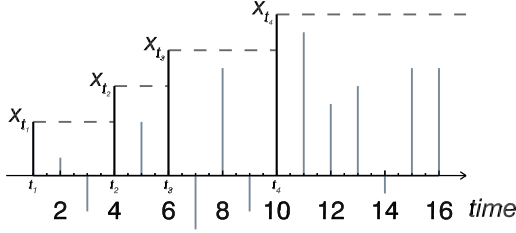


Figure 1. Illustration on the definition of records in a realization $\{x_i\}_{i=1,\dots,R}$ of the process $\{X_i\}_{i=1,\dots,R}$. Four records (black), $r_1 = x_{t_1=1}$, $r_2 = x_{t_2=4}$, $r_3 = x_{t_3=6}$, $r_4 = x_{t_4=10}$, are identified in the shown fragment.

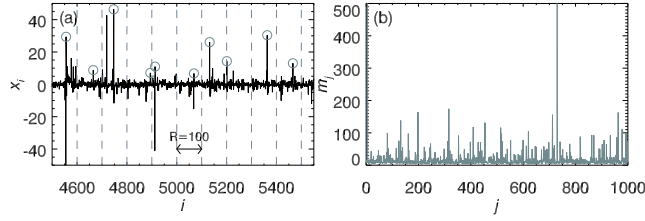


Figure 2. Definition of a sequence of block maxima $m_j = \max\{x_{jR}, \dots, x_{j(R+1)-1}\}_{j=0,1,\dots,[N/R]-1}$ [partially shown in (b)] by considering disjunct blocks of size $R = 100$ in the underlying time series $\{x_i\}_{i=0,1,\dots,N-1}$ [partially shown in (a)].

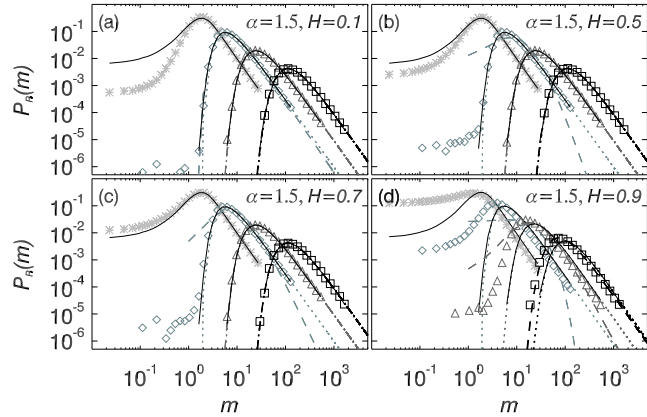


Figure 3. Probability density functions of block maxima for $\alpha = 1.5$ and different values of H and R . (a) and (b) are examples of anti-persistence while (c) and (d) correspond to examples of persistent behavior since $H = 1/\alpha = 2/3$ is the boundary between the two regimes. Shown are four different block sizes $R = 10$ [stars, light gray], $R = 100$ [diamonds, gray], $R = 1000$ [triangles, dark gray], and $R = 10000$ [squares, black]. The surrogate data for the corresponding independent SoS processes are indicated by solid black lines. Maximum-likelihood GEV fits are plotted as dotted curves (surrogate data) and dashed curves (original data) in the same gray tones for comparison.

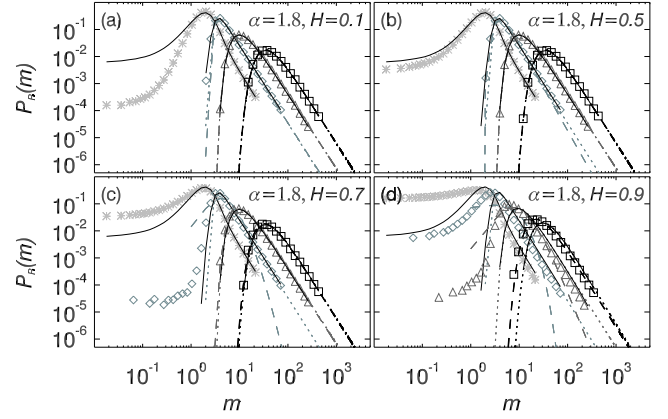


Figure 4. Same as Fig. 3 but for $\alpha = 1.8$. Note that now the independent case corresponds to $H = 1/\alpha = \frac{5}{9}$ and we have anti-persistence for $H < \frac{5}{9}$ and persistence for $H > \frac{5}{9}$. Thus, the persistence for $H = 0.9$ is stronger and the anti-persistence for $H = 0.1$ is weaker than in the case with $\alpha = 1.5$ shown in Fig. 3.

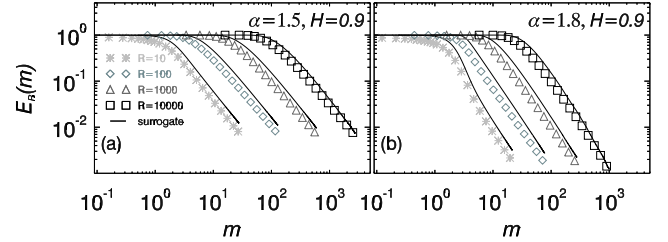


Figure 5. Exceedance probability, i. e., the probability to find an extreme event larger than m . Shown are results for self-similar SoS time series with $H = 0.9$ and the corresponding independent surrogates (black solid lines) for different block sizes R (symbols) and for different characteristic exponents (a) $\alpha = 1.5$ and (b) $\alpha = 1.8$.

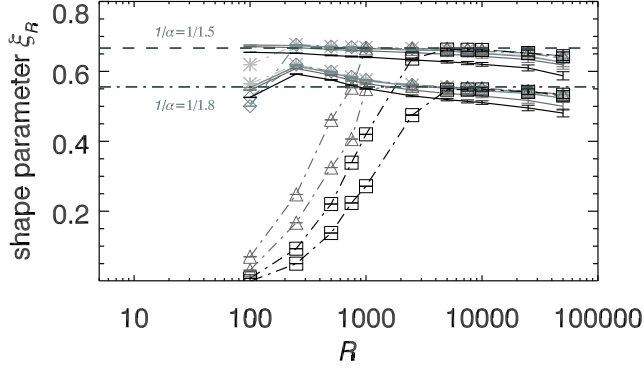


Figure 6. Convergence of the shape parameter ξ_R towards the theoretical value $1/\alpha$ as $R \rightarrow \infty$ obtained from GEV fits for four different self-similar SaaS time series [gray-scale coded dash-dotted lines and symbols] and corresponding independent surrogates [solid lines in same gray] — $H=0.1$ [light gray, stars], $H=0.2$ [gray, diamonds], $H=0.8$ [dark gray, triangles], and $H=0.9$ [black, squares]. Upper curves correspond to $\alpha = 1.5$ while lower curves belong to $\alpha = 1.8$. Error bars are 95%-confidence intervals of ξ_R obtained from the GEV fit after combining the data of all 1500 configurations.

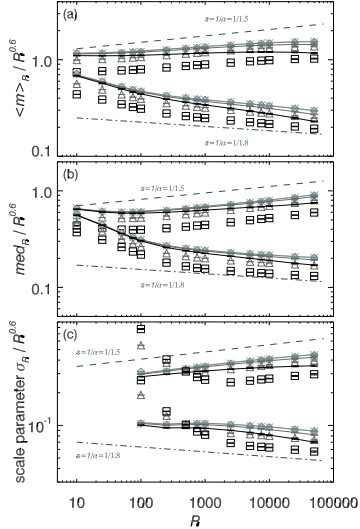


Figure 7. Dependence of (a) the mean $\langle m \rangle_R$ and (b) the median med_R block maximum together with (c) the scale parameter σ_R from a GEV fit on the block size R . Shown are results for four different self-similar SaaS time series [gray-scale coded symbols] and corresponding independent surrogates [solid lines in same gray tones] — $H=0.1$ [light gray, stars], $H=0.2$ [gray, diamonds], $H=0.8$ [dark gray, triangles], and $H=0.9$ [black, squares]. Upper curves belong to $\alpha = 1.5$ and lower curves to $\alpha = 1.8$. Shown are averages of $\langle m \rangle_R$ and med_R obtained separately for each configuration ($N_{\text{conf}} = 1500$) together with the ensemble standard deviations as error bars in (a,b). Expected rescaling exponents are indicated by dashed and dash-dotted lines, respectively. Note that the y-axis was rescaled by $R^{0.6}$ to enhance differences. Error bars in (c) are 95%-confidence intervals of σ_R obtained from a GEV fit after combining all N_{conf} configurations to increase statistics for large R .

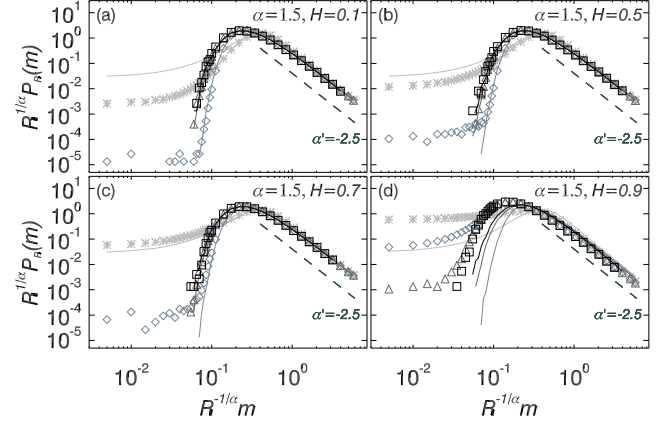


Figure 8. Rescaled versions of probability density functions shown in Fig. 3; the same gray tones and symbols are used. The expected asymptotic scaling of the tails is indicated by the dark gray dashed lines ($\alpha' = -1 - \alpha = -2.5$).

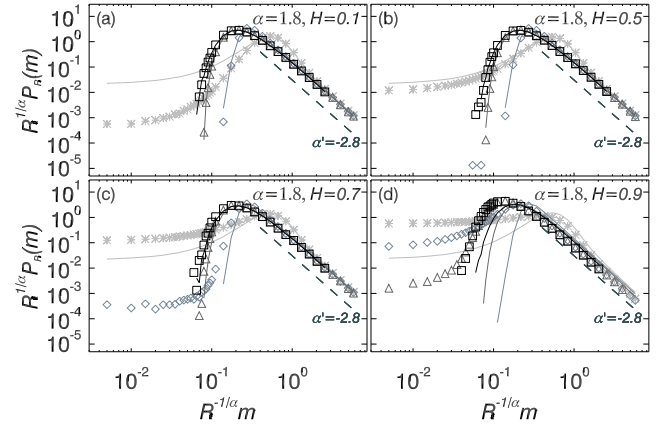


Figure 9. Same as Fig. 8 but for $\alpha = 1.8$.

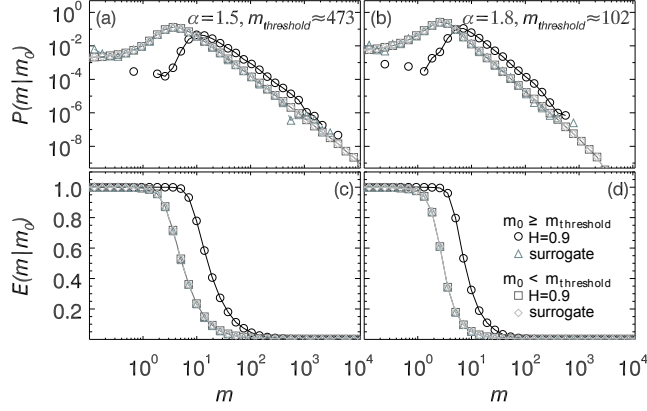


Figure 10. Examples of the conditional probability density functions for block maxima (a,b) and corresponding exceedances (c,d) for $R = 100$. Left panels (a,c) refer to $\alpha = 1.5$ and right panels (b,d) to $\alpha = 1.8$. Shown are results for block maxima m that are preceded by a block maximum $m_0 \geq m_{\text{threshold}}$ for a (large) self-similarity index $H = 0.9$ [black circles] and for the corresponding randomized sequence of block maxima [gray triangles]. For comparison results for the complementary condition $m_0 < m_{\text{threshold}}$ are also displayed (self-similar S α S processes [dark gray squares], independent surrogate [light gray diamonds]). The threshold has been chosen to ensure 15000 conditional maxima [(a,c) $m_{\text{threshold}} \approx 473$, (b,d) $m_{\text{threshold}} \approx 102$].

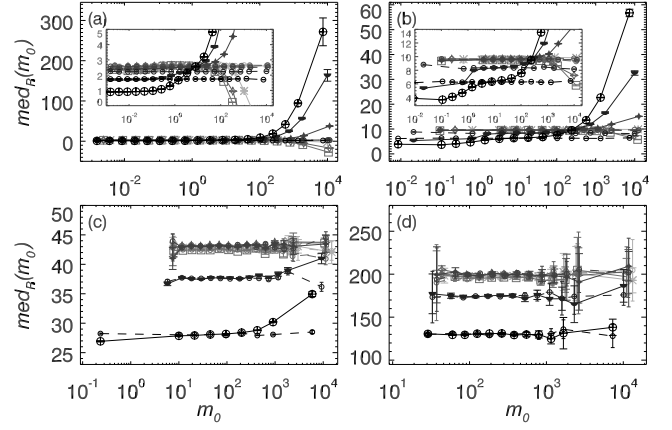


Figure 11. Median of the conditional distribution of block maxima, $\text{med}_R(m_0)$, given a preceding block maximum of m_0 for $\alpha = 1.5$. Results for different block sizes (a) $R = 10$, (b) $R = 100$, (c) $R = 1000$, (d) $R = 10000$ are shown. Different self-similarity exponents are both gray tone- and symbol coded; $H = 0.1$ [very light gray, stars], $H = 0.5$ [light gray, squares], $H = 0.6$ [gray, open diamonds], $H = 0.7$ [dark gray, filled diamonds], $H = 0.8$ [very dark gray, filled lower half circles], $H = 0.9$ [black, circles with plus]. The values expected in the absence of memory effects between block maxima are shown in the same gray-scale coding but with smaller open circles (see text for details). Note that both corresponding curves for data with and without memory must intersect. Error bars are obtained from bootstrapping [Efron, 1979; Efron and Tibshirani, 1993] within each bin: We draw the same number of elements as in the bin with a cap at 50000 and consider 10000 realizations per bin. The insets in (a,b) show magnifications of the intersection area.

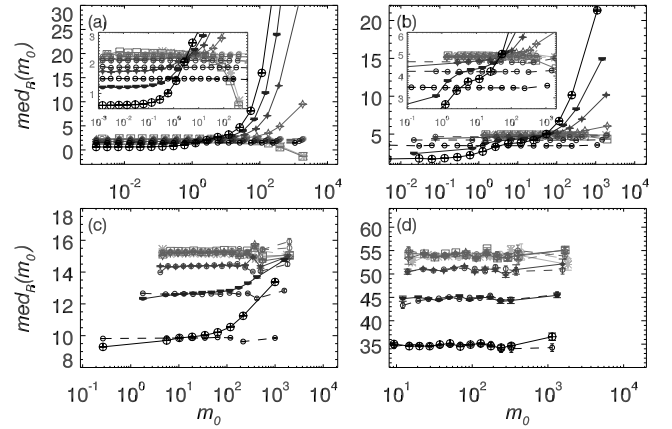


Figure 12. Same as Fig. 11 but for a characteristic exponent $\alpha = 1.8$. The main panels have the same x -axes as in Fig. 11 to allow a better comparison.

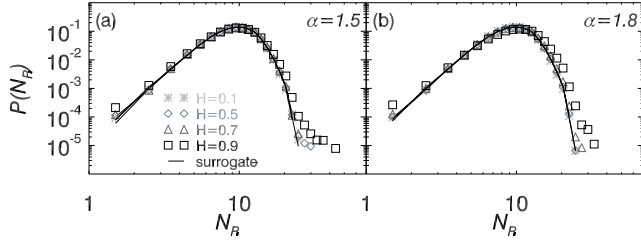


Figure 13. Probability of finding a given total number of records in sequences of block size $R = 10000$ for self-similar SaaS processes with different parameters α and H (symbols). Results for corresponding surrogate data are shown for comparison (lines).

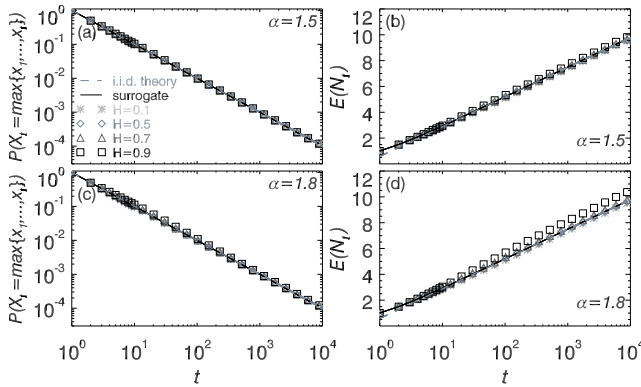


Figure 14. (a,c) Probability to break a record at a time t for different values of H and α . Black solid lines correspond to independent surrogate data ($H = 1/\alpha$) which don't deviate significantly from the theoretically expected $P(X_t = \max\{x_1, \dots, x_t\}) = 1/t$ — see Eq. (5). (b,d) Expected total number of records $E(N_t)$ that occur up to time t in the same color- and symbol coding as in (a,c). The theoretical iid behavior is $E(N_t) = \ln|t| + \gamma$; see Eq. (6a). Significant deviations from the iid behavior are visible in the presence of strong persistence ($H = 0.9$, $\alpha = 1.8$).

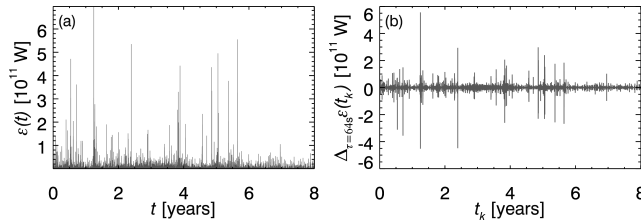


Figure 15. (a) Akasofu's $\epsilon(t)$ time series derived from ACE data according to Eq. (15) for the years 2000 to 2007 with a sampling of 64s. (b) $\Delta_{\tau=64s}\epsilon(t_k)$ time series obeying a symmetric heavy tailed distribution as shown by Moloney and Davidsen [2010].

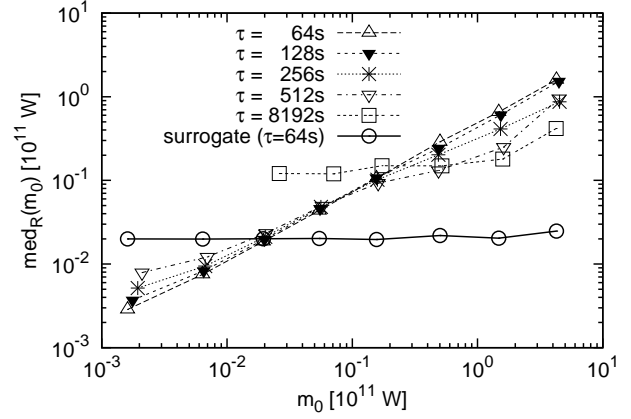


Figure 16. Median of the conditional distribution of block maxima $\text{med}_R(m_0)$ given a preceding block maximum of m_0 within a logarithmic bin for the $\Delta_{\tau}\epsilon$ series with different values of τ [symbols and line style coded]. The block size is $R = 100$. Surrogate data (obtained by shuffling the $\Delta_{\tau}\epsilon = 64s$ series' block maxima) corresponding to the iid case are shown for comparison [solid curve, circles]. Surrogates for other values of τ (not shown) are similar but increase monotonically with τ .

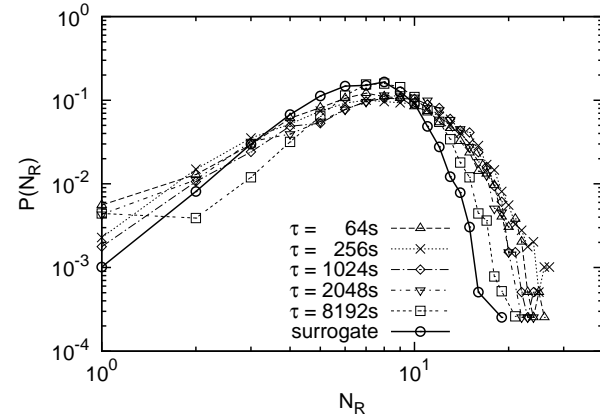


Figure 17. Probability density function for the number of records in non-overlapping blocks of size $R = 1000$ of the $\Delta_{\tau}\epsilon$ series for different values of τ and for surrogate data (obtained by shuffling the $\Delta_{\tau}\epsilon$ series) corresponding to the iid case are shown for comparison.

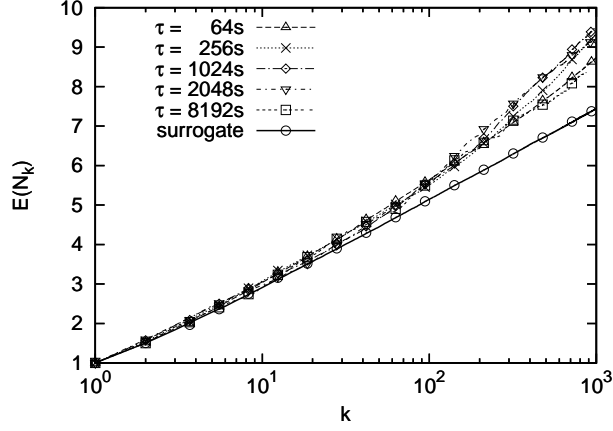


Figure 18. Expected number of records as a function of values k for the $\Delta_\tau \epsilon$ series for different values of τ . Estimates are based on non-overlapping blocks of size $R = 1000$. Surrogate data (obtained by shuffling the $\Delta_\tau \epsilon$ series) corresponding to the iid case are shown for comparison.

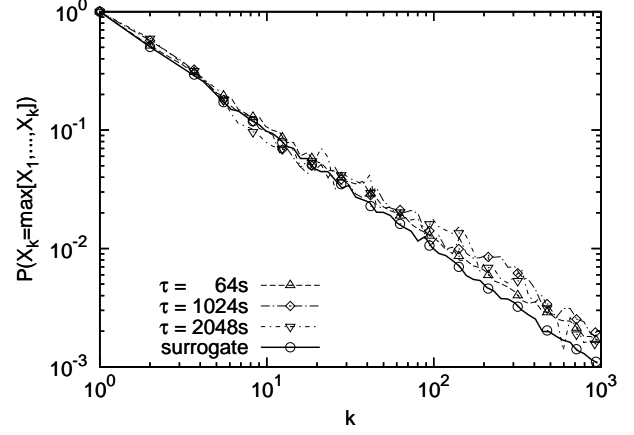


Figure 19. Probability to observe a record at values k for the $\Delta_\tau \epsilon$ series for different values of τ . Estimates are based on non-overlapping blocks of size $R = 1000$. Surrogate data (obtained by shuffling the $\Delta_\tau \epsilon$ series) corresponding to the iid case are shown for comparison.

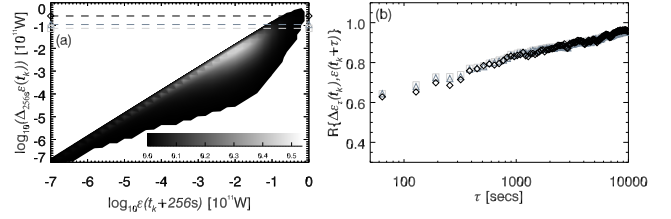


Figure 20. (a) Probability density function to observe a given pair of values $\epsilon(t_k + \tau)$ and $\Delta_\tau \epsilon(t_k) = \epsilon(t_k + \tau) - \epsilon(t_k)$ simultaneously for a fixed value of $\tau = 256$ s and only for pairs where $\Delta_\tau \epsilon(t_k) > 0$; logarithmic bins were used. The dashed lines indicate from top to bottom the 99.9% [black, diamonds], 99.5% [gray, triangles], and the 99% [light gray, squares] quantile of the $\Delta_{256s} \epsilon$ distribution. (b) Pearson's correlation coefficient calculated for the same upper quantiles as in (a) [same symbols and gray tones] for all time series pairs $(\Delta_\tau \epsilon(t_k), \epsilon(t_k + \tau))$ as a function of the time shift τ .